A Geometric Approach for Wave Propagation in 2-D Photonic Crystals in the Frequency Domain

P. Bettini, S. Boscolo, R. Specogna, and F. Trevisan

Department of Ingegneria Elettrica, Gestionale e Meccanica, Università di Udine, I-33100 Udine, Italy

We propose a pair of discrete geometric formulations to model two-dimensional (2-D) photonic crystals. Photonic crystals are periodic materials able to guide light by Bragg's reflection. We compared the results with an independent approach based on the multiple-scattering technique (MST).

***Index Terms*—Discrete approaches, photonic crystals, wave propagation.**

I. Introduction

PHOTONIC crystals consist of a periodic arrangement of dielectric or metallic elements [1] able to suppress the propagation of electromagnetic field in the structure for a given range of frequencies, i.e., the range of a complete *photonic bandgap*, [2], [3]. By introducing defects into the periodic lattice, we obtain a waveguide for light.

The aim of this paper is to model photonic crystals using the so-called discrete geometric approach based on the geometric structure behind Maxwell's equations [4]–[6].

We modeled the photonic crystal using a two-dimensional (2-D) geometry, and we will compare the results from the geometric approach with those from an independent approach based on the multiple-scattering technique (MST) [7].

II. Maxwell's Laws at Discrete Level

In the 2-D domain of interest D, we introduce a pair of interlocked cell complexes. One complex is made of simplexes (the 2-cells are triangles), while its dual is obtained from it, according to the barycentric subdivision. We indicate with $\mathcal{K}$ the primal complex (whose cells are endowed with *inner* orientation) and with $\tilde{\mathcal{K}}$ the dual (whose cells are endowed with *outer* orientation) [4]. As the same geometric element of a complex can be thought with two complementary orientations, we may construct the pair of meshes $\mathcal{M}' = (\mathcal{K}^s, \tilde{\mathcal{K}})$ and $\mathcal{M}'' = (\mathcal{K}, \tilde{\mathcal{K}}^s)$, where the suffix "$s$" indicates the simplicial complex. For brevity, we will indicate with $\mathcal{M}$, either $\mathcal{M}'$ or $\mathcal{M}''$.

We may model the electromagnetic field quantities in terms of differential p-forms [5]. Then, we consider the *de Rham map*, a machinery that integrates p-form ω with respect to the p-cells of mesh $\mathcal{M}$, yielding the degree of freedom (DoF) array $\boldsymbol{\omega}$, whose elements are indexed over the corresponding p-cells. We obtain that $\mathbf{U}$ is the DoF array of electromotive force (emf) associated with primal edges e, $\boldsymbol{\Phi}$ and $\mathbf{I}_m$ are the DoF arrays of induction fluxes and of the so-called magnetic currents associated with primal faces f, $\mathbf{F}$ is the DoF array of magnetomotive force (mmf) associated with dual edges $\tilde{e}$, $\boldsymbol{\Psi}$ and $\mathbf{I}_e$ are the DoF arrays of electric fluxes and of electric currents associated with dual faces $\tilde{f}$.

In our 2-D wave propagation problem, no free charge is present in D, and all the media are linear. The discrete Maxwell's equations written with respect to mesh $\mathcal{M}$ are

$$\mathbf{C}\mathbf{U} = -\mathbf{I}_m - d_t\boldsymbol{\Phi} \tag{1a}$$

$$\tilde{\mathbf{C}}\mathbf{F} = \mathbf{I}_e + d_t\boldsymbol{\Psi} \tag{1b}$$

$$\mathbf{D}\boldsymbol{\Phi} = 0 \tag{1c}$$

$$\tilde{\mathbf{D}}\boldsymbol{\Psi} = 0 \tag{1d}$$

where $\tilde{\mathbf{C}} = \mathbf{C}^T, \mathbf{D}$, and $\tilde{\mathbf{D}}$ are the usual incidence matrices defining interconnections between the cells of each complex forming $\mathcal{M}$. Continuity equation $\tilde{\mathbf{D}}(\mathbf{I}_e + d_t\boldsymbol{\Psi}) = 0$ is implied by (1b); from it and (1d), we have $\tilde{\mathbf{D}}\mathbf{I}_e = 0$.

Discrete laws (1b) are fulfilled exactly, while discrete constitutive laws between the DoF arrays

$$\mathbf{F} = \boldsymbol{\nu}\boldsymbol{\Phi} \tag{2a}$$

$$\boldsymbol{\Psi} = \varepsilon\mathbf{U} \tag{2b}$$

hold only approximately; these equations can also be written in an equivalent way as

$$\boldsymbol{\Phi} = \boldsymbol{\mu}\mathbf{F} \tag{3a}$$

$$\mathbf{U} = \zeta\boldsymbol{\Psi} \tag{3b}$$

where $\boldsymbol{\nu}$ and ε- or $\boldsymbol{\mu}$ and ζ- are some square mesh and medium dependent matrices.

III. Discrete Wave Propagation Problem

The discrete wave propagation problem consists of determining the arrays $\boldsymbol{\Phi}, \mathbf{U}, \mathbf{F}$, and $\boldsymbol{\Psi}$ such that (1) and (2)- or equivalently (3)- are satisfied simultaneously. Sources are specified as impressed electric currents $\mathbf{I}_e$ or as impressed magnetic currents $\mathbf{I}_m$ in a subregion D_s of D. Initial and boundary conditions have to be specified in addition. Along the boundary of D, an uniaxial perfectly matched layer (PML) of cells is considered [8].

A. Formulation in Terms of $\mathbf{U}$

In the case of a transverse-electric (TE)-field mode—the electric field is normal to the symmetry plane—it is convenient to refer to the mesh $\mathcal{M}'$, and we may reformulate the wave propagation problem in terms of DoF array $\mathbf{U}$, assuming the magnetic currents null in D_s. Then, by substituting in (1b), (2a) for $\mathbf{F}$, (2b) for $\boldsymbol{\Psi}$, and using (1a), we obtain

$$\left(\tilde{\mathbf{C}}'\boldsymbol{\nu}\mathbf{C}' + d_t^2\boldsymbol{\varepsilon}\right)\mathbf{U} = -d_t\mathbf{I}_e. \tag{4}$$

Digital Object Identifier 10.1109/TMAG.2006.872035

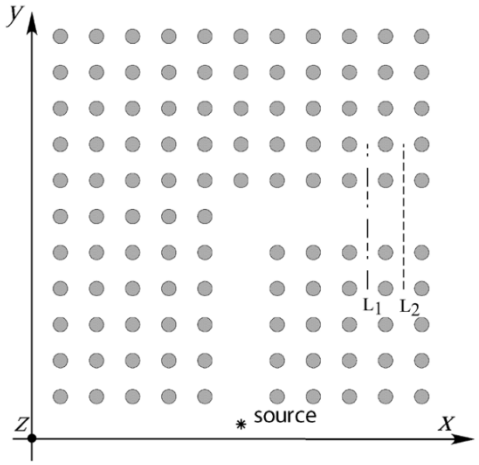

Fig. 1. Geometry of the plane model for the photonic crystal. The electric (magnetic) current source is also shown, together with line 1 (dashed–dotted) and 2 (dashed) used for numerical results comparison.

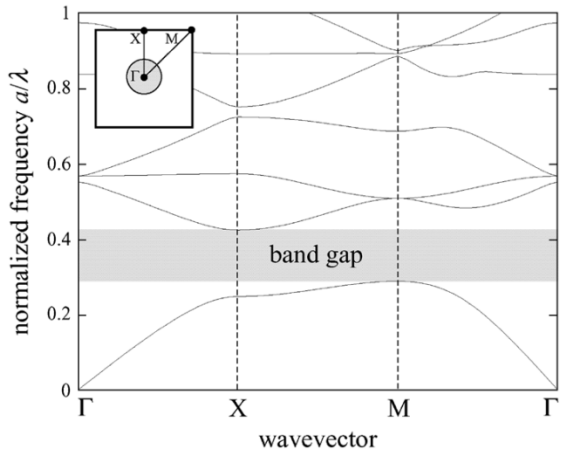

Fig. 2. TE band structure of a square lattice of dielectric pillars ($n_{\rm d} = 3.4, r/a = 0.2$) embedded in air. The elementary cell is schematized in the inset.

B. Formulation in Terms of $\mathbf{F}$

In the case of the transverse-magnetic (TM)-field mode—the magnetic field is normal to the symmetry plane—we consider the DoF array $\mathbf{F}$, and we assume the electric currents null in D_s. In this case, it is convenient to consider mesh $\mathcal{M}''$ and substituting in (1a), (3b) for $\mathbf{U}$, (3a) for $\mathbf{\Phi}$, and using (1b), we have

$$(\mathbf{C}''\boldsymbol{\zeta}\tilde{\mathbf{C}}'' + d_t^2\boldsymbol{\mu})\mathbf{F} = -d_t\mathbf{I}_m. \tag{5}$$

IV. Constitutive Matrices

Constitutive matrices $\boldsymbol{\nu}$ and $\boldsymbol{\varepsilon}$ for the formulation in terms of $\mathbf{U}$ on mesh $\mathcal{M}'$ can be easily derived in a geometric way. Matrix $\boldsymbol{\nu}$ is obtained by particularizing for triangles the idea developed in [9] for tetrahedra. On the other hand, with the electric field being normal to the symmetry plane, matrix $\boldsymbol{\varepsilon}$ has exactly the same geometric structure of the so-called Ohm's matrix described in [10], by simply swapping conductivity with permeability ε.

It is important to note here that due to the complementarity of the orientations of the same cell in $\mathcal{M}'$ and in $\mathcal{M}''$, we have that $\tilde{\mathbf{C}}'' = \mathbf{C}'$ and $\mathbf{C}'' = \tilde{\mathbf{C}}'$ hold. Therefore, the constitutive matrices $\boldsymbol{\zeta}, \boldsymbol{\mu}$ in (5) coincide with matrices $\boldsymbol{\nu}, \boldsymbol{\varepsilon}$ in (4), respectively, provided that we swap the material constants ν with $\zeta = 1/\varepsilon$ and ε with μ. This property allows us to unify the coding for the pair of formulations in terms of $\mathbf{U}$ or of $\mathbf{F}$ indifferently.

V. Model of the Test Geometry

As test geometry, we consider (Fig. 1) a square array of infinitely long dielectric pillars (refractive index $n_{\rm d} = 3.4$ and radius to pitch ratio $r/a = 0.2$) embedded in air, with a sharp 90° bend obtained by removing a line of pillars from the square lattice.

The *bandgaps* for the square lattice can be found by solving an eigenvalue problem on the borders of the irreducible Brillouin zone ΓXM [1], formulated as

$$\nabla \times \left[\frac{\nabla \times}{n^2(\boldsymbol{r})}\right]\boldsymbol{H}(\boldsymbol{r}) = \left(\frac{\omega}{\mathrm{c}_0}\right)\boldsymbol{H}(\boldsymbol{r}) \tag{6}$$

where $\boldsymbol{H}(\boldsymbol{r})$ is the magnetic field complex vector, ω is the angular frequency, $n(\boldsymbol{r})$ is the refractive index, and c_0 is the velocity of light in vacuum. Eigenvalues $\boldsymbol{H}(\boldsymbol{r})$ are the field patterns of the harmonic modes and the eigenvalues $(\omega/\mathrm{c}_0)^2$ are proportional to the squared frequencies of the modes.

It is a known result that only the TE-polarization exhibits a bandgap (see Fig. 2) in the range $0.28 < a/\lambda < 0.42$, where λ is the wavelength in the vacuum.

VI. Numerical Results

Numerical simulations for both the proposed formulations (4) and (5) have been carried out at a normalized frequency $a/\lambda = 0.32$ for TE and TM configurations.

As the square lattice of high-index pillars embedded in air exhibits a bandgap only for the TE polarization, we may expect a guided propagation throughout the waveguide only for such a polarized field.

In order to compare results, an independent approach, based on the MST, has been used to provide the reference data for both field configurations.

A. Multiple-Scattering Technique

The scattered field is calculated by expanding the field in cylindrical harmonics and by exploiting the continuity conditions on the surfaces of the pillars, thus not requiring any domain discretization and adsorbing boundary conditions.

Let us consider the case of a TE-polarized incident field and assume to have only the mth cylinder. When the sources are assigned in the substrate, we know the incident field $\boldsymbol{E}^i$ generated in the absence of the cylinders. As the incident field impinges on the cylinder, a scattered field $\boldsymbol{E}^s$ defined in the substrate and a field $\boldsymbol{E}^c$ transmitted into the cylinder appear. The scattered field and the field transmitted into the cylinder are defined in two homogenous regions, and admit the following modal solutions:

$$E_z^s = \sum_{\ell=-\infty}^{+\infty} b_{m,\ell} H_\ell^{(2)}(k_s r_m)\mathrm{e}^{i\ell\theta_m} \tag{7}$$

$$E_z^c = \sum_{\ell=-\infty}^{+\infty} c_{m,\ell} J_\ell(k_p r_m)\mathrm{e}^{i\ell\theta_m} \tag{8}$$

where r_m and θ_m are cylindrical coordinates centered in the cylinder center (x_m, y_m), and $k_m = 2\pi n_m/\lambda$ is the propa-

gation constant in the cylinder. Moreover $H^{(2)}(\cdot)$ in (7) is a second-type Hankel function.

In order to easily express the continuity condition on the cylinder boundary, we express the incident field E_z^i in terms of the following Fourier–Bessel: expansion

$$E_z^i = \sum_{\ell=-\infty}^{+\infty} a_{m,\ell} J_\ell(k_s r_m) \mathrm{e}^{i\ell\theta_m}. \tag{9}$$

Using Maxwell's equations and from (9), (7), and (8), it follows that the θ components of the incident, scattered, and transmitted magnetic fields, respectively, are

$$H_\theta^i = -\frac{i}{\mu r_m} \sum_{\ell=-\infty}^{+\infty} a_{m,\ell} k_s J'_\ell(k_s r_m) \mathrm{e}^{i\ell\theta_m}$$

$$H_\theta^s = -\frac{i}{\mu r_m} \sum_{\ell=-\infty}^{+\infty} b_{m,\ell} k_s H'^{(2)}_\ell(k_s r_m) \mathrm{e}^{i\ell\theta_m}$$

$$H_\theta^c = -\frac{i}{\mu r_m} \sum_{\ell=-\infty}^{+\infty} c_{m,\ell} k_p J'_\ell(k_p r_m) \mathrm{e}^{i\ell\theta_m}.$$

Finally, by writing the continuity conditions

$$\begin{cases} E_z^i + E_z^s = E_z^c \\ H_\theta^i + H_\theta^s = H_\theta^c \end{cases} \quad \text{in } r_m = R_m$$

we obtain, for the mth cylinder, the scattering matrix $\mathbf{S}_m$ whose coefficients are

$$s_{m\ell} = \frac{k_m J'_\ell(k_m R_m) J_\ell(k_s R_m) - k_s J'_\ell(k_s R_m) J_\ell(k_m R_m)}{k_s H'^{(2)}_\ell(k_s R_m) J_\ell(k_m R_m) - k_m J'_\ell(k_m R_m) H^{(2)}_\ell(k_s R_m)}.$$

The scattering matrix $\mathbf{S}_m$ is diagonal and depends only on the parameters R_m and n_m of the mth cylinder. It links the coefficients of the locally scattered field and those of the locally incident field with the matrix relation

$$\boldsymbol{b}_m = \mathbf{S}_m \boldsymbol{a}_m \tag{10}$$

where we denoted by $\boldsymbol{a}_m$ and $\boldsymbol{b}_m$ the column vectors of coefficients $a_{\ell,m}$ and $b_{\ell,m}$, respectively.

For more than one cylinder, we simply superimpose the effects, and from (10), we have

$$\boldsymbol{b}_p = \mathbf{S}_m \left(\boldsymbol{a}_m + \sum_{n \neq m} \mathbf{T}_{mn} \boldsymbol{b}_n \right) \tag{11}$$

where $\boldsymbol{a}_m$ represents the local contribute due to the incident field, and the term $\mathbf{T}_{mn}\boldsymbol{b}_n$ represents the field scattered by the nth cylinder in the direction of the mth cylinder, thus acting as a secondary incident field for this cylinder. In order to write relation (11), we have to express the field $\boldsymbol{E}_n^s$ scattered by the nth cylinder in the coordinate reference of the mth cylinder. Graf's formula [11, eq. (9.1.79)] solves this point by giving for the matrices $\mathbf{T}_{mn}$ the following expression:

$$\mathbf{T}_{mn}(j,\ell) = H^{(2)}_{\ell-j}(k_s d_{nm}) \mathrm{e}^{\mathrm{i}(\ell-j)\theta_{nm}}$$

where d_{nm} is the distance between the centers of cylinders m and n, and θ_{nm} is the azimuthal coordinate of cylinder n in the reference frame of cylinder m, respectively.

By moving all the terms related to scattered fields to the left side in (11), we obtain the linear system of equations

$$\boldsymbol{b}_m - \sum_{n \neq m} \mathbf{S}_m \mathbf{T}_{mn} \boldsymbol{b}_n = \mathbf{S}_m \boldsymbol{a}_m.$$

If the square and column submatrices $\mathbf{S}_m, \mathbf{I}, \mathbf{T}_{mn}, \boldsymbol{b}_m$, and $\boldsymbol{a}_m$ are truncated in order to keep the indices ℓ and j between $-L$ and $+L$, the final size of the system to be solved is $N(2L+1)$.

Finally by solving the linear system, the total electric field E_z outside the cylinders can be written as

$$E_z = E_z^i + \sum_{m=1}^{N} \sum_{\ell=-L}^{+L} b_{m,\ell} H^{(2)}_\ell(k_s r_m) \mathrm{e}^{i\ell\theta_m}. \tag{12}$$

B. Geometric Approach

To solve the 2-D wave propagation problem, when the electric field is normal to the plane of symmetry (TE configuration, $\boldsymbol{E} = E_z \hat{\boldsymbol{z}}$), we used formulation (4) on $\mathcal{M}'$, while the complementary case of the electric field on the symmetry plane (TM configuration, $\boldsymbol{H} = H_z \hat{\boldsymbol{z}}$) is solved with formulation (5) on $\mathcal{M}''$.

The volumes of meshes $\mathcal{M}'$ or $\mathcal{M}''$ are prisms with triangular base (on the plane of symmetry) and unitary height. In both the formulations, the DoF are attached to the edges normal to the symmetry plane (having unitary height) and thence one-to-one with the nodes of the 2-D triangular mesh (we used 155 000 triangles).

Along the boundary of domain D an uniaxial PML of cells is considered to avoid reflections. Unfortunately, a wide number (20 layers) of PML elements along the boundary is necessary to reach a high level of accuracy, but it greatly worsens the conditioning of the problem and raises the computational cost of numerical solution, even though an efficient iterative algorithm (based on CG from NAG Scientific Library) is adopted to solve (4) or (5), for the TE or TM cases, respectively.

In the numerical analysis, an elementary electric or magnetic current source, parallel to the cylinder axes, is placed in the middle of the input port of the waveguide, as in Fig. 1, for a TE- or TM-polarized field, respectively.

The results of the analysis carried out with the geometric approach are presented in Fig. 3 (TE configuration) and in Fig. 4 (TM configurations) from a qualitative point of view. As expected, a guided propagation throughout the structure is obtained only for a TE-polarized field, as can be seen in Fig. 4. The numerical results obtained with the discrete geometric method for TE configuration are compared with those from the MST in the spectral domain, at normalized frequency $a/\lambda = 0.32$, in terms of normalized amplitude and phase of the electric field at selected points of lines L1 and line L2 of Fig. 1, as reported in Figs. 5 and 6.

The agreement is very good in both cases. However, it must be pointed that a careful optimization of PML parameters is required to reach an acceptable compromise between accuracy and computational cost of the numerical solution of the problem.

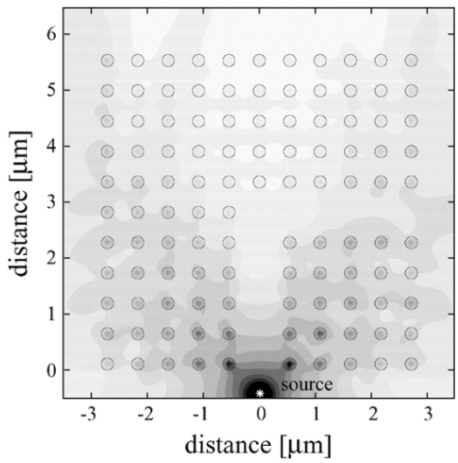

Fig. 3. TM polarization: Amplitude of the magnetic field $\boldsymbol{H} = H_z\hat{z}$.

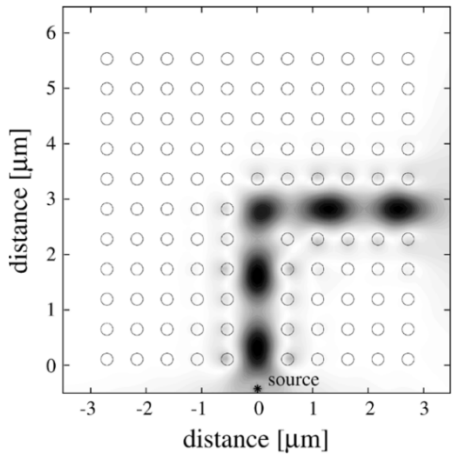

Fig. 4. TE polarization: Amplitude of the electric field $\boldsymbol{E} = E_z\hat{z}$.

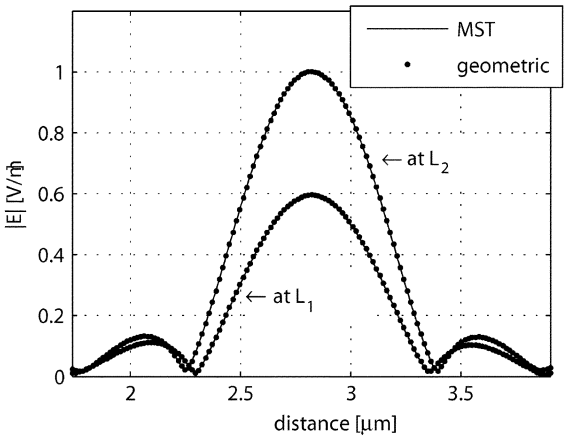

Fig. 5. Amplitude of the electric field ($\mathbf{E} = E_z\hat{\mathbf{z}}$ component) at the output cross section: Lines L_1 and L_2 of Fig. 1.

VII. Conclusion

A pair of discrete geometric formulations to model 2-D photonic crystals in the frequency domain has been developed and the numerical results for a selected geometry compared with those from an independent approach based on the MST. The analysis performed with the two methods show an excellent agreement that evidences a difference lower than −100 dB between the calculations in the worst case. On the other hand, the geometric approach required a high number of triangles to accurately model the geometry of the photonic crystal. Correspondingly, we had to consider up to 20 layers of PML elements along the boundary, worsening the conditioning of the problem.

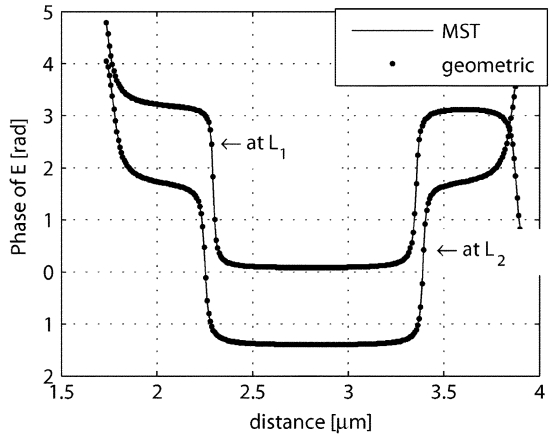

Fig. 6. Phase of the electric field ($\mathbf{E} = E_z\hat{\mathbf{z}}$ component) at the output cross section: Lines L_1 and L_2 of Fig. 1.

References

[1] J. D. Joannopoulos, R. D. Meade, and J. N. Winn, *Photonic Crystals*. Princeton, NJ: Princeton Univ. Press, 1995.

[2] E. Yablonovitch, "Photonic band-gap structures," *J. Opt. Soc. Amer. B*, vol. 10, pp. 283–295, 1993.

[3] P. R. Villeneuve and M. Piché, "Photonic bandgaps in periodic dielectric structures," *Prog. Quantum Electron.*, vol. 18, pp. 153–200, 1994.

[4] E. Tonti, "Algebraic topology and computational electromagnetism," in *Proc. 4th Int. Workshop Electric Magnetic Field*, Marseille, France, May 12–15, 1988, pp. 284–294.

[5] A. Bossavit and L. Kettunen, "Yee-like schemes on staggered cellular grids: A synthesis between FIT and FEM approaches," *IEEE Trans. Magn.*, vol. 36, no. 4, pp. 861–867, Jul. 2000.

[6] T. Tarhasaari and L. Kettunen, "Wave propagation and cochain formulations," *IEEE Trans. Magn.*, vol. 39, no. 3, pp. 1195–1198, May 2003.

[7] G. Tayeb and D. Maystre, "Rigorous theoretical study of finite-size two-dimensional photonic crystals doped by microcavities," *J. Opt. Soc. Amer. A*, vol. 14, pp. 3323–3332, 1997.

[8] J. B. Bérenger, "A perfectly matched layer for the absorption of electromagnetic waves," *J. Comput. Phys.*, vol. 114, no. 1, pp. 185–200, 1994.

[9] F. Trevisan and L. Kettunen, "Geometric interpretation of discrete approaches to solving magnetostatics," *IEEE Trans. Magn.*, vol. 40, no. 2, pp. 361–365, Mar. 2004.

[10] F. Bellina, P. Bettini, E. Tonti, and F. Trevisan, "Finite formulation for the solution of a 2D eddy-current problem," *IEEE Trans. Magn.*, vol. 38, no. 2, pp. 561–564, Mar. 2002.

[11] M. Abramowitz and I. Stegun, *Handbook of Mathematical Functions*. New York: Dover, 1964.

Manuscript received June 20, 2005 (e-mail: trevisan@uniud.it).